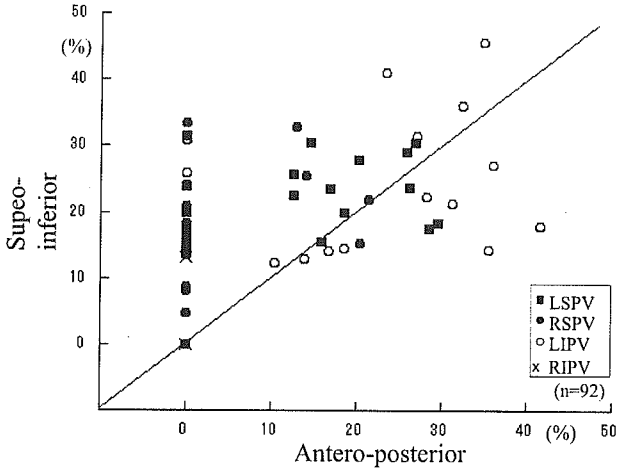

Figure 5. *Relationship between the percent reduction of the supero-inferior diameter and the antero-superior diameter of the PV after ablation. The abbreviations are the same as in Figure 4.*

Changes in the LA and Relationship to the PVs After Ablation

The LA diameters after ablation were smaller than those before ablation ($P < 0.005$, for each; Table I). The supero-inferior percent diameter reduction of the ostium in the ablated PVs ($r = 0.30$, $P < 0.005$), as well as in the nonablated PVs ($r = 0.53$, $P < 0.05$), correlated with the supero-inferior percent diameter reduction of the LA. The reductive luminal alteration at the ablation site derived from the estimated ablation site before ablation (average, 23 ± 15%; range, −5% to 65%) correlated not only with the supero-inferior percent diameter reduction inside the PV ($r = 0.46$; $P < 0.001$) but also with the percent diameter reduction of the LA ($r = 0.43$; $P < 0.001$).

Discussion

Major Findings

The quantitative analysis of the PV morphology performed by CT in this study demonstrated the following novel findings. (1) Shrinkage of the PV trunk was often observed in the ablated PVs, and its severity did not correlate with the changes in the LA diameter but did with the severity of the *de novo* PV narrowing. (2) After ablation, the reduction in the diameters of both the PV ostium and the ablation site in the ablated veins, as well as the reduction in the diameter of the PV ostium in the nonablated PVs, correlated with the reduction in the diameter of the LA after ablation. (3) Luminal reduction inside the PV after ablation occurred in a bidirectional manner, and its severity was usually greater in the supero-inferior direction than in the antero-posterior direction, with 60% of PV narrowing detected only in the supero-inferior direction. No *de novo* PV narrowing had a diameter reduction ≥25% only in the antero-posterior

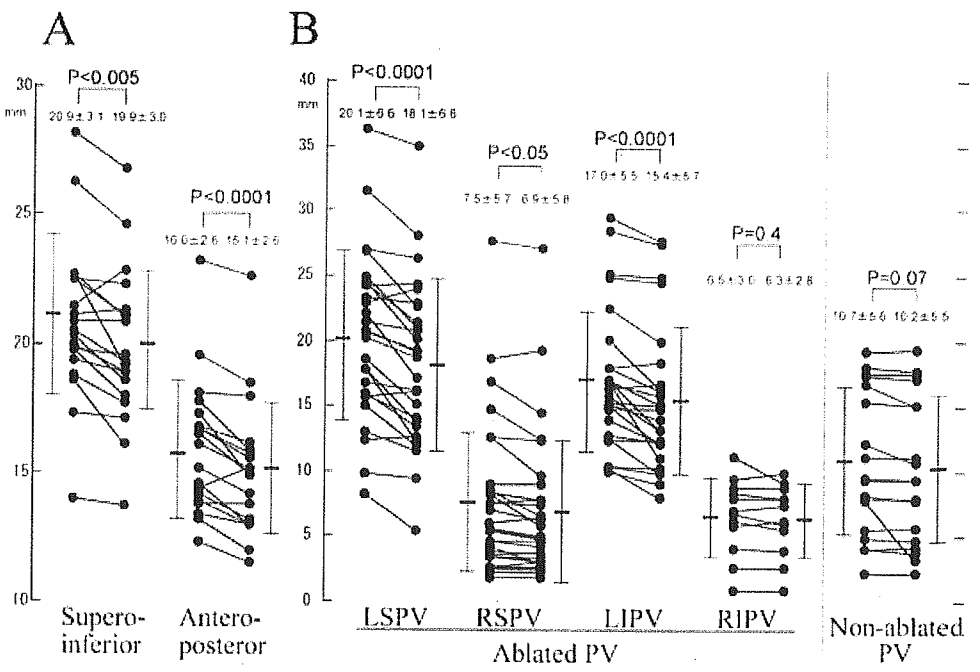

Figure 6. *(A) Changes in the supero-inferior and antero-posterior ostial diameters of the non-ablated pulmonary veins (PVs). (B) Changes in the trunk length of the ablated and non-ablated PVs. The abbreviations are the same as in Figure 4.*

direction. (4) Narrowing of the PV was found in about 10% of PVs in the patients with AF before ablation as well as in the control subjects, and it was most often found in the LIPV. No pre-existent narrowing had a diameter reduction ≥25% only in the supero-inferior direction.

These findings indicate that an asymmetric bidirectional luminal reduction and longitudinal shrinkage of the PV are characteristic morphologic changes after ablation. Structural and reverse remodeling of the PV together with the LA remodeling may affect the changes in the PV diameter. Bidirectional viewing before and after ablation is preferable to avoid missing a pre-existent lesion or underestimating the asymmetric bidirectional reduction within the PV. Meanwhile, only bidirectional viewing after ablation can distinguish a unidirectional narrowing that can be sporadically encountered, between one that is a *de novo* narrowing located only in the supero-inferior direction, and one that is a pre-existent narrowing located only in the antero-posterior direction.

Pattern and Proposed Mechanism of the Morphologic Changes in the PVs After Ablation

A recent study demonstrated that fibrocellular intimal proliferation, endovascular contraction, and elastic proliferation were responsible for PV narrowing more than 6 weeks after RF energy applications, and that endovascular contraction was observed typically at the site at which the RF energy application produced necrosis with a resulting scar formation.[10] In the present study, shrinkage of the PV trunk after ablation was not influenced by the changes in the LA size but by the severity of the PV narrowing at the ablation sites. Therefore, endovascular contraction caused by RF energy deliveries within the proximal portion of the PV might cause a longitudinal shrinkage of the PV trunk as well as PV stenosis.

The muscle sleeve over the proximal portion of the PV is distributed heterogeneously, which is predominantly in the inferior portion of the superior PVs and in the superior portion of the inferior PVs.[11] A recent study also demonstrated that the sites with electrical breakthroughs where RF energy delivery impaired the conduction between the LA and the PV were often located at the superior and inferior segments within the PV.[12] In keeping with a heterogeneous distribution of the myocardial sleeve within the proximal PV and to isolate the PV electrically from the LA, RF energy has to be applied more often at the superior and inferior segments than at the anterior and posterior segments within the PV, which may result in heterogeneous PV stenosis.

Proposed Mechanism of the Narrowing Within the Nonablated PVs

Dense fibrous connective tissue around the distal portion of the myocardial sleeve from the LA into the PV has been reported.[13] We hypothesized that the dense fibrous tissue representing the histological junction between the LA and the proper PV involving medial smooth muscle forms a pre-existent mild luminal reduction in the PV at the vicinity of the ostium. In addition, as Figure 2B shows, adjacency to the descending aorta may be associated with the greatest frequency of narrowing in the LIPV. In patients with pectus excavatum, a kinking of the LIPV has been reported.[14] The specific location of the vein lying between the LA and the spine may be related to the narrowing of the LIPV in this group (Fig. 2C).

Reverse Remodeling After PV Isolation in the PVs and LA

A decrease or elimination of the recurrence of AF has been expected to develop "reverse remodeling" of the LA and PVs, resulting in restoration of the enlarged dimensions. However, few studies have ever characterized the reverse remodeling of the PVs or the relationship between the LA and the PVs after ablation. In the present study, we demonstrated that dilated PV ostia in both non-ablated and ablated PVs are reduced after ablation, and that the reduction in the diameter of the PV ostium correlates with that of the LA after ablation. These findings indicate that reverse remodeling of the PVs can occur after successful ablation and is observed with a reduction in the LA size. In addition to the histological changes caused by the RF energy delivery, reverse remodeling of the PVs may play an important role in the reduction of the diameter at the ablation site after ablation. The present study and a previous study demonstrated no significant difference in the PV trunk between the AF and the control subjects.[7] Meanwhile, Kato et al. reported that the PV trunk of the AF group was significantly larger than that of the control subjects.[5] The difference in the results among the three studies was supposedly due to undisclosed differences in the characteristics, i.e., physical size or gender of the control subjects.

Imaging and Measurements

In previous articles, the severity of the reduction inside the PV was determined quantitatively using a unidirectional view. Further, a measurement or estimation of the diameter at the ablation site before ablation was not sufficiently

attempted.[4–6] The curved MPR is a kind of three-dimensional reconstruction that allows for an integrated oblique view encompassing the whole PV lumen, trunk and branches, and has been available for quantitative evaluation of stenosis of the coronary arteries.[9,15] In the present study, we measured the PV diameters in two orthogonal directions and estimated the diameter at the ablation site in consideration of the longitudinal shrinkage retrospectively using curved MPR.

Limitations

A limitation of this study was that the extensive shrinkage might have complicated the estimation of the luminal reduction or alteration in the PVs because of an underestimation of the reference diameters or deformation of the ostia. A second limitation was that we could not completely distinguish a *de novo* luminal reduction from a pre-existent luminal reduction. Third, in the present study, no clinical stenosis of the PVs occurred after ablation. Thus, we cannot assert whether or not unidirectional viewing missed in any way any clinical PV stenosis after ablation. Finally, the distance between the ablation site and the ostium was calculated on the assumption of a linear relationship between the trunk length and the luminal reduction of the PVs, and this assumption might not have been the case. However, as mentioned in the "Results" section, the percent shortening of the trunk length demonstrated a significant linear relationship to the luminal reduction. Therefore, we believe that the error range was very small and made no difference in the results.

References

1. Haissaguerre M, Shah DC, Jais P, et al. Electrophysiological breakthroughs from the left atrium to the pulmonary veins. Circulation 2000; 102:2463–2465.
2. Oral H, Knight BP, Tada H, et al. Pulmonary vein isolation for paroxysmal and persistent atrial fibrillation. Circulation 2002; 105:1077–1081.
3. Robbins IM, Colvin EV, Doyle TP, et al. Pulmonary vein stenosis after catheter ablation of atrial fibrillation. Circulation 1998; 98:1769–1775.
4. Scharf C, Sneider M, Case I, et al. Anatomy of the pulmonary veins in patients with atrial fibrillation and effects of segmental ostial ablation analyzed by computed tomography. J Cardiovasc Electrophysiol 2003; 14:150–155.
5. Kato R, Lickfett L, Meininger G, et al. Pulmonary vein in patients undergoing catheter ablation of atrial fibrillation: Lessons learned by use of magnetic resonance imaging. Circulation 2003; 107:2004–2010.
6. Dill T, Neumann T, Ekinci O, et al. Pulmonary vein diameter reduction after radiofrequency catheter ablation for paroxysmal atrial fibrillation evaluated by contrast-enhanced three-dimensional magnetic resonance imaging. Circulation 2003; 107:845–850.
7. Schwartzman D, Lacomis J, Wigginton WG. Characterization of left atrium and distal pulmonary vein morphology using multidimensional computed tomography. J Am Coll Cardiol 2003; 41:1349–1357.
8. Tada H, Oral H, Wasmer K, et al. Pulmonary vein isolation: Comparison of bipolar and unipolar electrograms at successful ostial ablation sites. J Cardiovasc Electrophysiol 2002; 13:13–19.
9. Ropers D, Baum U, Pohle K, et al. Detection of coronary artery stenoses with thin-slice multi-detector row spiral computed tomography and multiplanar reconstruction. Circulation 2003; 107:664–666.
10. Taylor GW, Kay GN, Zheng X, et al. Pathological effects of extensive radiofrequency energy applications in the pulmonary veins in dogs. Circulation 2000; 101:1736–1742.
11. Ho SY, Cabrera JA, Tran VH, et al. Architecture of the pulmonary veins: Relevance to radiofrequency ablation. Heart 2001; 86:265–270.
12. Yamane T, Shah DC, Jais P, et al. Electrogram polarity reversal as an additional indicator of breakthroughs from the left atrium to the pulmonary veins. J Am Coll Cardiol 2002; 39:1337–1344.
13. Saito T, Waki K, Becker AE. Left atrial myocardial extension onto pulmonary veins in humans: Anatomic observation relevant for atrial arrhythmias. J Cardiovasc Electrophysiol 2000; 11:888–894.
14. Takahashi K, Sugimoto H, Ohsawa T. Obliteration of the descending aortic interface in pectus excavatum: Correlation with clockwise rotation of the heart. Radiology 1992; 182:825–828.
15. Achenbach S, Ulzheimer S, Baum U, et al. Noninvasive coronary angiography by retrospectively ECG-gated multislice spiral CT. Circulation 2000; 102:2823–2328.

ELSEVIER

International Journal of Cardiology 103 (2005) 105–106

International Journal of Cardiology

www.elsevier.com/locate/ijcard

Letter to the Editor

Large collateral conus branch to the left anterior descending branch of the coronary artery in a subject with angina pectoris demonstrated by multislice computed tomography

Nobusada Funabashi*, Miki Asano, Issei Komuro

Department of Cardiovascular Science and Medicine, Chiba University Graduate School of Medicine, 1-8-1 Inohana, Chuo-ku, Chiba City, Chiba 260-8670, Japan

Received 20 March 2004; accepted 17 June 2004
Available online 5 February 2005

A 70-year-old male presented to our hospital for chest pain. To evaluate the coronary arteries, electrocardiogram-gated enhanced multislice computed tomography (CT) (Light Speed Ultra, General Electric, Milwaukee, WI, USA) was performed with a 1.25-mm slice thickness, helical pitch 3.25. Thirty seconds after intravenous injection of 100 ml of iodinated contrast material (350 mgI/ml), CT scanning was performed with retrospective ECG-gated reconstruction and volume data were transferred to a workstation (Virtual Place Office Azemoto Tokyo Japan).

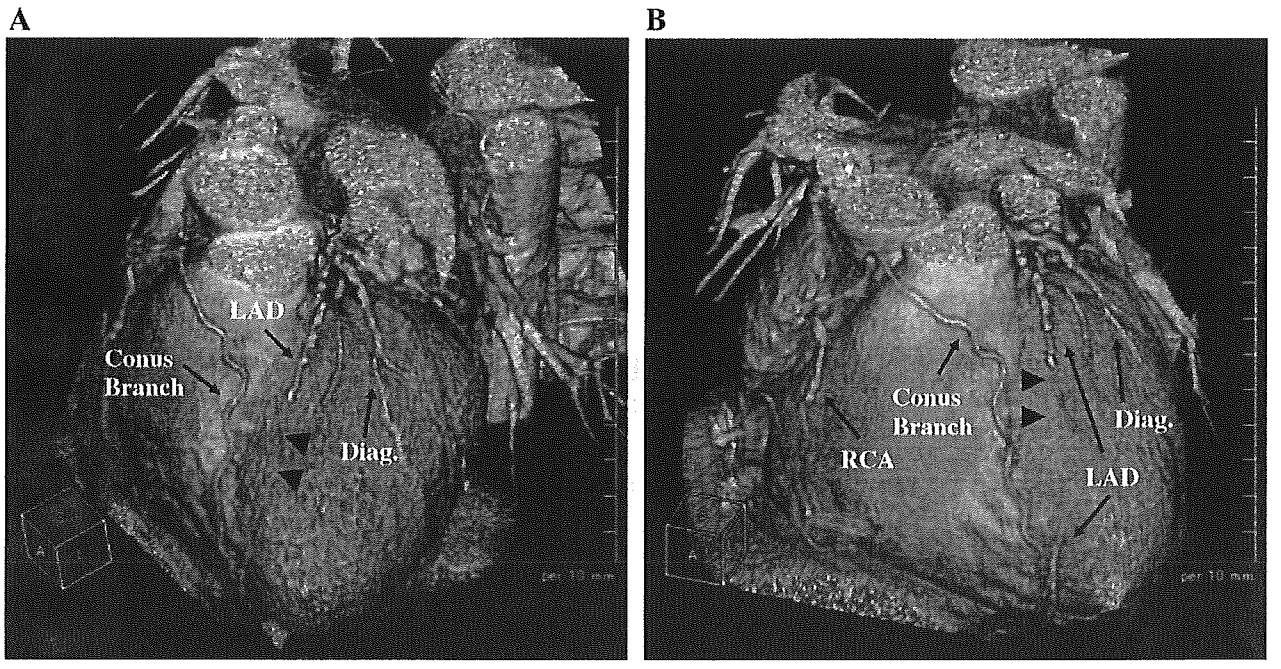

Fig. 1. Three dimensional volume-rendering images of enhanced electrocardiogram-gated multislice computed tomography revealed total occlusion of the left anterior descending branch (LAD) (arrowheads) and a large conus branch originating from the right coronary artery (RCA) that fed into the distal part of the LAD. Diag. indicates diagonal branch.

* Corresponding author.
E-mail address: nobusada@ma.kcom.ne.jp (N. Funabashi).

0167-5273/$ - see front matter © 2005 Elsevier Ireland Ltd. All rights reserved.
doi:10.1016/j.ijcard.2004.06.017

Three dimensional volume-rendering images revealed total occlusion of the left anterior descending branch (LAD) (arrowheads, Fig. 1A,B) and a large conus branch originating from the right coronary artery (RCA) that fed into the distal part of the LAD. Conventional coronary angiograms revealed the same findings of total occlusion of the LAD (arrowheads, Fig. 2A) and a collateral conus branch originating from the RCA that fed into the distal part of the LAD (Fig. 2B). As blood flow of the collateral artery was good, normal motion of the left ventricle was revealed by a selective left ventriculogram, and his chest pain was improved by the oral administration of nitroglycerin and a β-blocker, no interventions were performed.

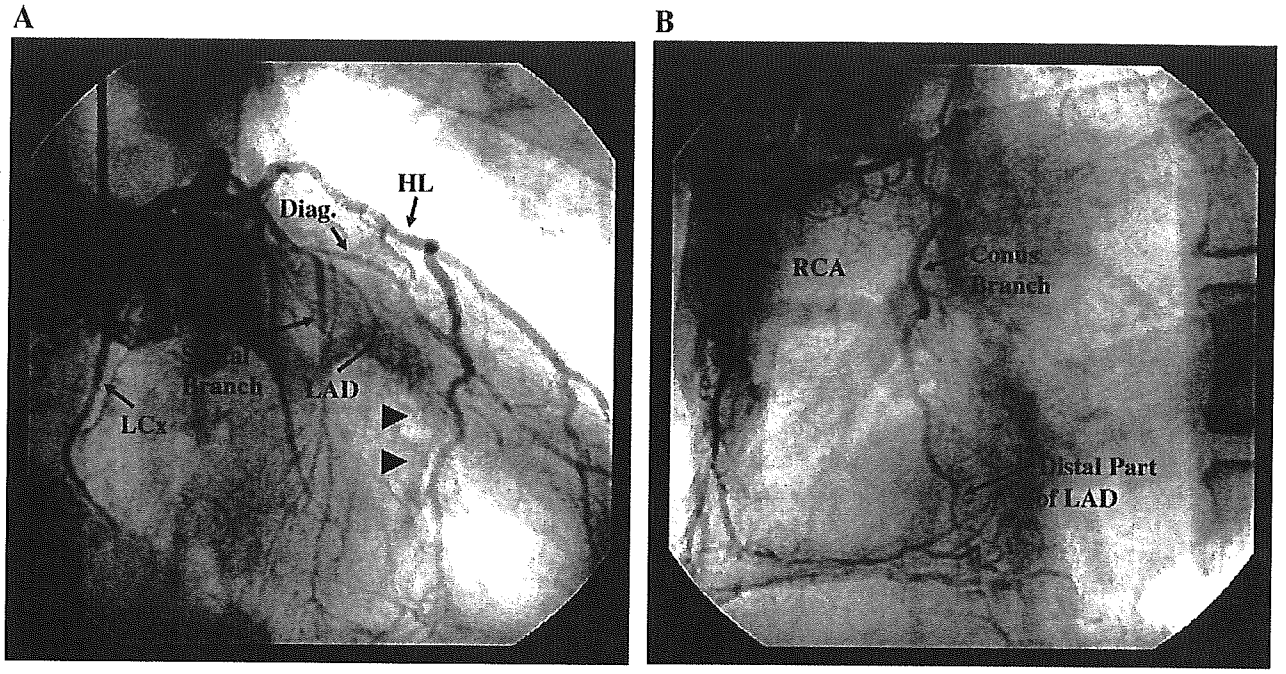

Fig. 2. Conventional coronary angiograms revealed the same findings of total occlusion of the LAD (arrowheads, A) and a collateral conus branch originating from the RCA that fed into the distal part of the LAD (B). Diag., HL, and LCx indicate diagonal branch, high lateral branch, and left circumflex branch, respectively.

ELSEVIER

International Journal of Cardiology 106 (2006) 270–272

International Journal of Cardiology

www.elsevier.com/locate/ijcard

Letter to the Editor

Atherosclerotic right internal thoracic arterial aneurysm demonstrated by multislice computed tomography

Yuriko Niitsuma[b], Nobusada Funabashi[a,*], Mizuho Imamaki[b], Issei Komuro[a], Masaru Miyazaki[b]

[a]*Department of Cardiovascular Science and Medicine, Chiba University Graduate School of Medicine, 1-8-1 Inohana, Chuo-ku, Chiba City, Chiba 260-8670, Japan*

[b]*Department of General Surgery, Chiba University Graduate School of Medicine, Chiba, Japan*

Received 30 October 2004; accepted 31 December 2004
Available online 1 April 2005

Keywords: Internal thoracic arterial aneurysm; Multislice computed tomography; Coronary artery bypass graft

A 74-year-old male presented with weight loss; stomach cancer was diagnosed that required surgery. As he had chest pains on effort, a conventional coronary angiogram was performed, which revealed severe stenosis of the left main branch, and a coronary artery bypass graft (CABG) was indicated.

Evaluation of the aorta and internal thoracic artery (ITA) was done using ECG-gated enhanced multislice computed tomography (CT) (Light Speed Ultra 16, General Electric, Milwaukee, Wisconsin) with a 1.25 mm slice thickness, helical pitch 6.00. CT scanning was performed 30 s after intravenous injection of 100 ml of iodinated contrast material (350 mgI/ml). Axial source (Fig. 1A) and sagittal view (Fig. 1B) of multiplanar reconstruction image and volume-rendered images (Fig. 1C and D), revealed normal findings except for a right ITA (RITA) aneurysm (arrowheads) and aortic arch calcification. The surgeons had planned to connect the left ITA to the left circumflex branch and, as stomach cancer precluded the use of the gastro-epiploic artery, they chose the RITA to connect to the left anterior descending (LAD) artery. During the CABG procedure the RITA aneurysm (10 mm in diameter) was resected (arrow Fig. 2A). The radial artery was connected to the proximal portion of the RITA and the radial arterial graft to LAD. Pathological examination of the resected aneurysm revealed plaque (★) with thickened intima, fragmentation of the membrane elastic interna (arrow) (Fig. 2B) and excessive cholesterin deposition in intima. Therefore the RITA aneurysm was considered due to atherosclerosis rather than specific arteritis or systemic connective tissue disease.

* Corresponding author. Tel.: +81 43 222 7171.
E-mail address: nobusada@ma.kcom.ne.jp (N. Funabashi).

0167-5273/$ - see front matter © 2005 Elsevier Ireland Ltd. All rights reserved.
doi:10.1016/j.ijcard.2004.12.081

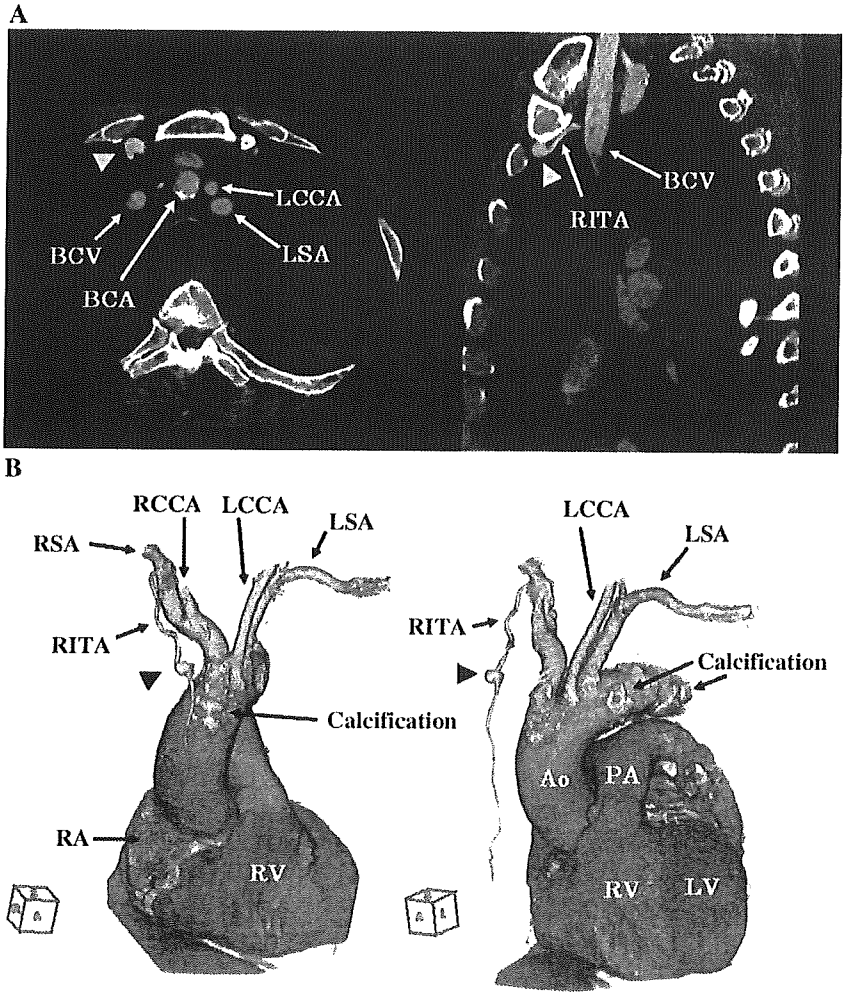

Fig. 1. A and B: Axial source (A) and sagittal view (B) of multiplanar images of enhanced electrocardiograph-gated multislice computed tomography show the aneurysm of the right internal thoracic artery (RITA) (arrowheads). (C) and (D) Volume-rendered images of enhanced electrocardiogram-gated multislice computed tomography show the aneurysm of the right internal thoracic artery (RITA) (arrowheads). Calcification of aortic arch can also be observed. BCV (brachiocephalic vein), BCA (brachiocephalic artery), LCCA (left common carotid artery), LSA (left subclavian artery), RSA (right subclavian artery), RCCA (right common carotid artery), RA (right atria), RV (right ventricle), Ao (aorta), PA (pulmonary artery), and LV (left ventricle).

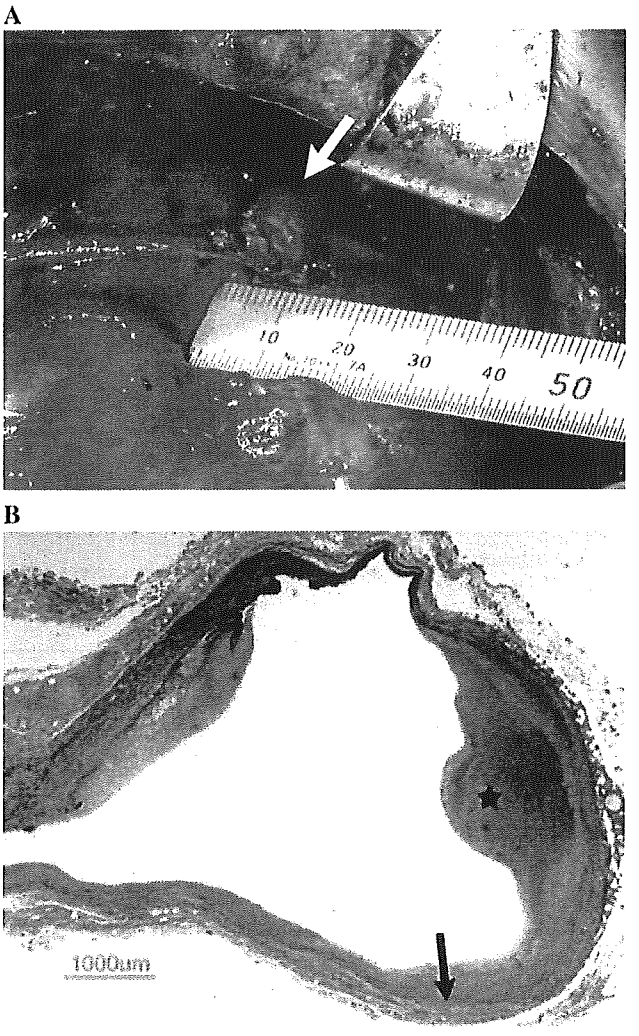

Fig. 2. (A) Intraoperative photograph of the aneurysm of the right internal thoracic artery (RITA) (arrow). (B) Histological section of the wall of the aneurysm of the RITA in Elastica van Gieson stein represented plaque (★) with thickened intima and fragmentation of the membrane elastica interna (arrow). Original magnification ×20.

ELSEVIER

International Journal of Cardiology 107 (2006) 130–131

International Journal of Cardiology

www.elsevier.com/locate/ijcard

Letter to the Editor

Patency of gastroepiploic arterial graft to left circumflex branch with distal portion of the anastomotic site demonstrated by multislice computed tomography

Nobusada Funabashi*, Issei Komuro

Department of Cardiovascular Science and Medicine, Chiba University Graduate School of Medicine, Chiba University Hospital, 1-8-1 Inohana, Chuo-ku, Chiba City, Chiba 260-8670, Japan

Received 2 January 2005; accepted 6 January 2005
Available online 5 April 2005

A 77-year-old male presented to our hospital with chest pain on effort 5 years previously. Conventional coronary angiogram (CAG) revealed occlusion in the proximal left circumflex branch (LCx) and right coronary artery (RCA), with distal collateral arteries and occlusion of the ostium of the left subclavian artery (LSA). He underwent a coronary artery bypass connecting the aortic root to the mid portions of the RCA using a saphenous vein graft (SVG), and a gastroepiploic arterial (GEA) graft to the distal LCx. An artificial graft was also implanted from the ascending aorta to the mid portion of the LSA. Postoperatively, CAG revealed a patent GEA graft but completely occluded ostium of the SVG. Five years later, although asymptomatic, electrocardiogram (ECG)-gated enhanced multislice computed tomography (CT) (Light Speed Ultra 16, General Electric, Milwaukee, WI) was performed with 1.25-mm slice thickness, helical pitch 6.00. Thirty seconds after intravenous injection of 100 ml of iodinated contrast material (350 mg/ml), CT scanning was performed with retrospective ECG-gated reconstruction and volume data were transferred to a workstation (Virtual Place Office Azemoto, Tokyo).

Volume-rendered images revealed occlusion of the LSA and patent mid and distal portions fed by the artificial graft (Fig. 1A,B). The SVG was completely occluded at the ostium. The proximal LCx was occluded and the distal portion of the anastomotic site of the GEA graft was visualized (arrowheads Fig. 2A,B), findings identical to the previous CAG.

* Corresponding author.
E-mail address: nobusada@ma.kcom.ne.jp (N. Funabashi).

0167-5273/$ - see front matter © 2005 Elsevier Ireland Ltd. All rights reserved.
doi:10.1016/j.ijcard.2005.01.049

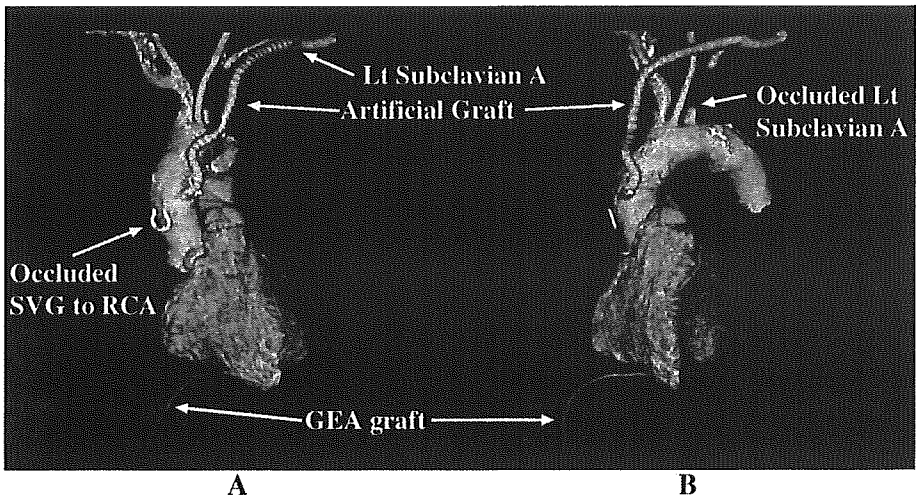

Fig. 1. Volume-rendered images of enhanced ECG-gated multislice computed tomography from the anterior view (A) and left anterior view (B) revealed the occluded proximal portion of the left subclavian artery (Lt Subclavian A), and the mid and distal portions of the Lt Subclavian A fed by the artificial graft from the ascending aorta with good patency. The saphenous vein graft (SVG), which should have connected to the right coronary artery (RCA), was completely occluded at the ostium of the graft. The gastroepiploic arterial (GEA) graft could also be visualized.

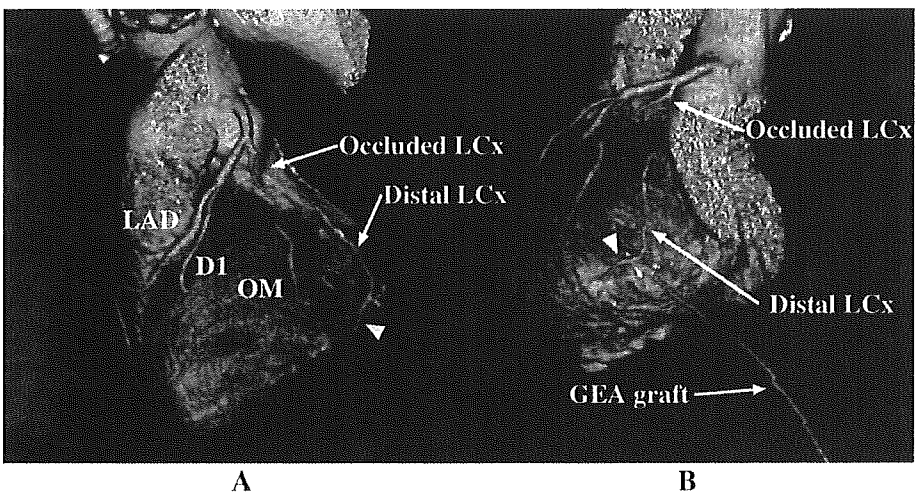

Fig. 2. Volume-rendered images of enhanced ECG-gated multislice computed tomography from the left superior posterior view (A) and posterior view (B) revealed that the proximal portion of the left circumflex branch (LCx) was occluded. The GEA graft was connected to the distal portion of the LCx and the distal portion of the anastomotic site of the GEA graft was visualized (Arrowheads). LAD, D1, and OM indicate left anterior descending branch, 1st diagonal branch, and obtuse marginal branch, respectively.

Enhanced Functional Gap Junction Neoformation by Protein Kinase A–Dependent and Epac-Dependent Signals Downstream of cAMP in Cardiac Myocytes

Satoshi Somekawa, Shigetomo Fukuhara, Yoshikazu Nakaoka, Hisakazu Fujita, Yoshihiko Saito, Naoki Mochizuki

Abstract—Gap junctions (GJs) constituted by neighboring cardiac myocytes are essential for gating ions and small molecules to coordinate cardiac contractions. cAMP is suggested to be a potent stimulus for enhancement of GJ function. However, it remains elusive how cAMP potentiates the GJ of cardiomyocytes. Here we demonstrated that the gating function of GJ is enhanced by the protein kinase A (PKA)–dependent signal, and that the accumulation of connexin43 (Cx43), the most abundant Cx in myocytes, is enhanced by an exchange protein directly activated by cAMP (Epac) (Rap1 activator)–dependent signal. The gating function of GJs was analyzed by microinjected dye transfer method. The accumulation of Cx43 was analyzed by quantitative immunostaining. Using the PKA-specific activator N^6-benzoyladenosine-3′,5′-cyclic monophosphate (6Bnz) and Epac-specific activator 8-(4-chlorophenylthio)-2′-*O*-methyladenosine-3′,5′-cyclic monophosphate (8CPT), we could delineate the two important downstream signals of cAMP for enhanced GJ neoformation. Whereas 6Bnz potentiated gating function of GJs with slight accumulation of Cx43 at cell–cell contacts, 8CPT remarkably enhanced the accumulation of Cx43 with a slight effect on gating. We further noticed that adherens junctions (AJs) were maturated by 8CPT, as marked by increased neural-cadherin immunostaining. Because AJ formation precedes the GJ formation, AJ formation accelerated by Epac-Rap1 signal may result in enhanced GJ formation. The involvement of Epac-Rap1 signal in GJ neoformation was further confirmed by evidence that inactivation of Rap1 by overexpression of Rap1GAP1b perturbed the accumulation of Cx43 at cell–cell contacts. Collectively, PKA and Epac cooperatively enhance functional GJ neoformation in cardiomyocytes. (***Circ Res.* 2005;97:655-662.**)

Key Words: gap junction ■ connexin43 ■ myocardial structure ■ cardiac gap junction connexins

Gap junctions (GJs) are channels formed by two docking connexons; one connexon is provided by each of the two contiguous cells and is constituted of six connexin (Cx) molecules.[1] Among the 20 Cx members, Cx40, Cx43, and Cx45 are expressed in the heart.[2] Of the three, Cx43 is predominantly expressed in working heart muscle cells.[3,4] GJs in the heart are characterized by their localization at the intercalated disk between each myocyte and also by their role in electrical conductance required for coordinated electrical excitation.[5] Myocytes electrically coupled by GJs show synchronized contraction. The importance of Cx43 in electrical excitation in vivo is evident by cardiac-specific depletion of Cx43 leading to cardiac arrhythmia.[6]

The overall function of GJs depends on the number of GJs and the gating function of assembled GJs. GJs are upregulated by increased transcription of Cx, increased distribution of Cx at cell–cell contacts, and decreased degradation of Cx from the cell membrane. cAMP increases Cx43 mRNA,[7] cAMP also enhances the trafficking of Cx43 from the endoplasmic reticulum/Golgi apparatus to the plasma membrane.[8] Cx43 turnover is regulated by proteosomal and lysosomal degradation, and the half-life of Cx43 is less than two hours, suggesting that a rapid synthesis and trafficking system operates in cardiac myocytes.[9]

GJ is modulated by the phosphorylation of Cx43 on Ser and Tyr residues. The intercellular communication through Cx43 is decelerated and accelerated by its phosphorylation on Ser368 by protein kinase C and on Ser364 by protein kinase A (PKA), respectively.[10,11] In addition to Ser phosphorylation, phosphorylated Cx43 on Tyr247 and Tyr265 is repressed from junctional communication.[12] In addition to phosphorylation, GJ formation is regulated by Cx43-binding molecules. Cx43 binds to the junctional adhesion molecule-associating proteins zonula occludens-1 (ZO-1) and β-catenin.[13,14] Dominant-negative ZO-1, which dissociates the endogenous ZO-1 from Cx43, disturbs the localization of

Original received May 10, 2005; resubmission received July 12, 2005; revised resubmission received August 11, 2005; accepted August 16, 2005.
From the Department of Structural Analysis (S.F., Y.N., H.F., N.M.), National Cardiovascular Center Research Institute, Suita, Osaka; the First Department of Internal Medicine (S.S., Y.S.), Nara Medical University, Kashihara, Nara, Japan.
Correspondence to Naoki Mochizuki, Department of Structural Analysis, National Cardiovascular Center Research Institute, 5-7-1 Fujishirodai, Suita, Osaka 565-8565, Japan. E-mail nmochizu@ri.ncvc.go.jp
© 2005 American Heart Association, Inc.

Circulation Research is available at http://circres.ahajournals.org DOI: 10.1161/01.RES.0000183880.49270.f9

Cx43 at the cell–cell contacts, resulting in the reduced conductance of GJs.[13] Wnt-1 signal prevents β-catenin degradation, thereby increasing β-catenin, which not only drives Cx43 expression but also associates with the Cx43 at the cell–cell contacts, where β-catenin localizes with cadherin.[14]

cAMP-induced Cx43 assembly has been extensively characterized in terms of Cx43 synthesis, delivery to the plasma membrane, and phosphorylation, which is believed to depend exclusively on PKA.[15] However, other downstream molecules of cAMP have not been elucidated in the neoformation of GJs. We and others have demonstrated that exchange protein directly activated by cAMP (Epac)/cAMP-GEF, a guanine nucleotide exchange factor (GEF) for Rap1, is activated by cAMP,[16,17] and that cAMP–Epac-Rap1 signal enhances the barrier function of vascular endothelial cells by stabilizing cadherin-mediated cell adhesion.[18,19] Analogous to this Epac-induced cadherin-based cell adhesion, we hypothesized that Epac may be involved in GJ neoformation as a cAMP-triggered signaling molecule in cardiac myocytes.

In this study, we investigated the molecular mechanism by which GJ neoformation is regulated by cAMP using a PKA-specific activator and an Epac-specific activator. We analyzed the GJ accumulation at cell–cell contacts by immunostaining of Cx43 and the gating function of GJs by dye spreading in neonatal rat cardiomyocytes (NRCMs) stimulated with these activators. We demonstrate that the Cx43 accumulation at cell–cell contacts depends on Epac and that dye spreading depends on PKA. Therefore, PKA and Epac downstream of cAMP cooperatively enhance functional GJ neoformation in cardiac myocytes.

Materials and Methods

Reagents and cAMP Analogs

Dibutyryl-cAMP (dbcAMP) was purchased from Sigma-Aldrich, Epac-specific activator 8-(4-chlorophenylthio)-2′-*O*-methyladenosine-3′,5′-cyclic monophosphate (8CPT) from Calbiochem; and PKA-specific activator N^6-benzoyladenosine-3′,5′-cyclic monophosphate (6Bnz) was from BIOLOG Life Science Institute. Other chemical compounds, antibodies, and adenoviruses are listed in the supplemental information (available online at http://circres.ahajournals.org).

Cell Culture

NRCMs were isolated from Wistar rats (1 to 2 days old; Kiwa Jikken Dobutsu, Japan) on a Percoll gradient as described previously.[20] The details of cardiac myocyte preparation are described in the supplemental information. The NRCMs spread onto the glass-base dishes for 24 hours after isolation were subjected to immunostaining or dye transfer assay after drug treatment for another 12 hours. We observed that the adherens junctions (AJs) were not maturated, although NRCMs contacted each other before the drug treatment, indicating that we used the reassembling NRCMs for the experiments. Experiments using animals were approved by our institutional animal use and care committee. All animal procedures were performed according to the *Guide for the Care and Use of Laboratory Animals* (NIH, revision 1996).

Immunocytochemistry

NRCMs stimulated with cAMP analogs were immunostained as described previously.[21] Briefly, cells cultured on glass-base dish were blocked with PBS containing 4% BSA for 1 hour at room temperature (RT), then stained with anti-Cx43, anti–sarcomeric α-actinin (S-αA), and anti–neural (N)-cadherin at RT. Protein reacting with primary antibodies was visualized with Alexa 488–labeled goat anti-rabbit IgG and Alexa 546–labeled goat anti-mouse IgG. Images were recorded with a confocal microscope (BX50WI; Olympus). For quantitative immunofluorescence analysis, images were also recorded using an epifluorescence microscope (IX-71; Olympus) controlled by MetaMorph version 6.2 software (Molecular Devices). The number of Cx43-positive dots at the cell–cell contacts on the fluorescence images were counted as Cx43 puncta.

Gating Function of GJs Analyzed by Microinjected Dye Transfer

Microinjected dye transfer was performed as described by Doble et al, with minor modifications.[22] The details of dye transfer method are described in the supplemental information.

RT-PCR Analysis

Total RNAs extracted from NRCMs and human cervical carcinoma cell line (HeLa) cells using Trizol (Invitrogen) were reverse-transcribed using SuperScript II and random primers (Invitrogen). The resultant DNAs were PCR-amplified using Epac-specific primers described in the supplemental information.

Western Blot Analysis and N-Cadherin Translocation Assay

NRCMs were lysed in buffer described in the supplemental information. Lysates precleared by centrifugation at 15 000*g* for 10 minutes were subjected to SDS-PAGE and immunoblotting with antibodies as indicated in Figures 3, 4, 5, and 6. Proteins reacting with primary antibodies were visualized by an enhanced chemiluminescence system (Amersham Biosciences) with peroxidase-conjugated and species-matched secondary antibodies and analyzed with an LAS-1000 system (Fuji Film). N-cadherin translocation assay was performed as described previously.[18]

Detection of GTP-Bound Form of Rap1

Rap1 activity was assessed by a modified Bos method as described previously.[23] Briefly, NRCMs starved in DMEM for 3 hours were treated with the stimulants as indicated in Figures 3 and 6 and lysed at 4°C in a pull-down lysis buffer described in the supplemental information. GTP-bound Rap1 was collected on glutathione *S*-transferase fused with Rap1 binding domain of Ral guanine nucleotide dissociation stimulator precoupled to glutathione-Sepharose beads and subjected to SDS-PAGE followed by immunoblotting using anti-Rap1.

Statistical Analysis

The results were expressed as the mean±SD. Student *t* test was used to analyze differences between two groups. Group differences were assessed with one-way ANOVA or two-way ANOVA, followed by post hoc comparisons tested with Scheffe's method. At least 3 fields randomly selected from each culture for analysis of Cx43 staining or at least 4 cells for dye transfer assay from each culture were used to yield a single value for each culture. The number of the cultures for analysis was indicated in the figure legends as n. Significant differences were indicated as P value <0.05 (*).

Results

cAMP Enhances Functional GJ Neoformation in Cultured NRCMs

Because cAMP has been reported previously to enhance GJ formation,[7] we confirmed the dbcAMP–regulated functional GJ neoformation by quantitatively analyzing Cx43 accumulation at the cell–cell contacts by immunostaining and gating function of GJs by microinjected dye transfer assay. dbcAMP enhanced the Cx43 accumulation at the cell–cell contacts (Figure 1A and 1B). To neglect the possibility of cardiac fibroblast contamination in the NRCMs in the following

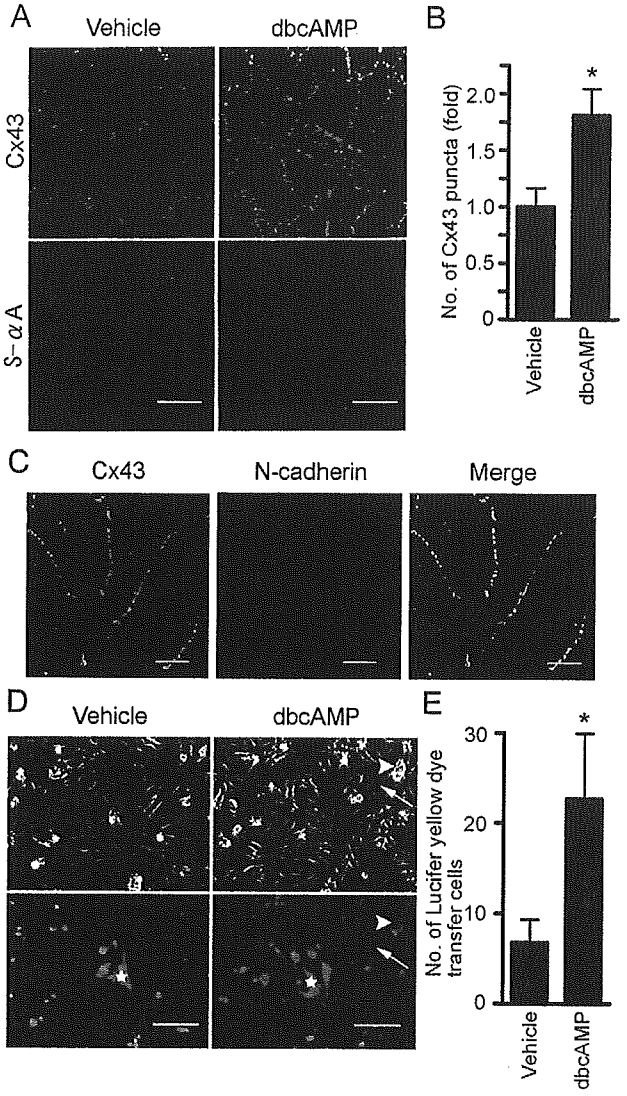

Figure 1. cAMP induces Cx43 accumulation at cell–cell contacts and enhances gap junctional intercellular communication. A, NRCMs cultured 24 hours after cell preparation were stimulated with vehicle or 1 mmol/L dbcAMP for 12 hours. Cells were stained with anti-Cx43 (green) and anti-S-αA (red). Images were obtained through a confocal microscope (BX50WI). Bar=20 μm. B, NRCMs stimulated by dbcAMP were analyzed for Cx43 accumulation by counting the number of puncta at cell–cell contacts. Mean number±SD is expressed as fold increase relative to that observed in the cell treated with vehicle. *$P<0.05$ vs vehicle as analyzed by Student's t test (n=4). Three fields randomly selected from each culture were used for measuring the fold activation between vehicle- and dbcAMP-treated culture by counting Cx43-positive puncta. C, Cells treated with dbcAMP were immunostained with anti-Cx43 (green) and anti–N-cadherin (red). A merged image is shown on the right. Note that puncta for Cx43 are localized to cell–cell contacts as indicated by the N-cadherin immunostaining. Bar=5 μm. D, Microinjected dye transfer assay shows the extent of dye transferring between neighboring cells through GJs. NRCMs stimulated with 1 mmol/L dbcAMP for 12 hours were microinjected with 10% Lucifer yellow. Cells 3 minutes after dye injection were phase contrast imaged (top panels) and fluorescence imaged (bottom panels). Asterisks indicate dye-injected cells. Arrows and arrowheads denote typical dye-transferred cell and cell debris emitting nonspecific fluorescence, respectively. Bar=50 μm. E, Quantitative analysis of D is shown as mean number of dye-positive cells in either vehicle or dbcAMP-treated NRCMs. *$P<0.05$ as analyzed by Student's t test (n=6).

experiments, and to show the confluence of the NRCMs, cells were immunostained for sarcomeric α-actinin (Figure 1A, bottom). The Cx43 puncta in the cells treated with dbcAMP for 12 hours were clearly observed at the cell–cell contacts, where N-cadherin localized (Figure 1C), indicating that dbcAMP induces the accumulation of Cx43 at the cell–cell contacts. We investigated the effect of dbcAMP on gating function of GJs by microinjected dye transfer assays (Figure 1D and 1E). Microinjected dye was more widely transferred to the neighboring cells in dbcAMP-treated NRCMs than vehicle-treated cells (Figure 1D). The quantitative data are shown in Figure 1E. These results are in agreement with previous reports[7,8] and validated the assays we used in this study.

PKA Is Required But Not Sufficient Alone for cAMP-Enhanced GJ Neoformation

Because PKA is involved in the enhancement of GJ formation,[15] we first tested the effect of H89, a specific PKA inhibitor, on cAMP-enhanced accumulation of Cx43. Unexpectedly, H89 did not block the dbcAMP-induced accumulation of Cx43 (Figure 2A and 2B), although H89 did block cAMP-enhanced intercellular communication assessed by microinjected dye transfer assays (Figure 2C).

We next examined the effect of 6Bnz, a specific activator for PKA,[24] on intercellular communication and Cx43 accumulation at cell–cell contacts to directly assess the involvement of PKA in cAMP-enhanced GJ formation. 6Bnz induced Cx43 accumulation slightly but to a much lesser extent than dbcAMP (Figure 2D and 2E). Notably, 6Bnz enhanced dye transfer to a greater extent than vehicle but to a lesser extent than dbcAMP (Figure 2F). These results indicate that PKA signaling is required but not sufficient alone for cAMP-enhanced GJ neoformation and suggest that there is a novel signaling downstream of cAMP in addition to PKA involved in Cx43 accumulation at cell–cell contacts for functional GJ neoformation.

cAMP Activates PKA and Epac-Rap1 Signaling in NRCMs

Epac has been identified as a novel cAMP target and a Rap1-specific GEF. We therefore hypothesized that Epac-Rap1 signaling may be involved in cAMP-enhanced GJ neoformation. RT-PCR analysis revealed the expression of Epac in NRCM but not in HeLa cells used as a negative control (Figure 3A). To test the hypothesis, we first examined whether dbcAMP induces the activation of Rap1 and the phosphorylation of cAMP response element binding protein (CREB) in NRCMs. As shown in Figure 3B, dbcAMP induced Rap1 and CREB activation in NRCMs. Rap1 activation by dbcAMP is dependent on time and concentration (supplemental Figure IA and IB, available online at http://circres.ahajournals.org). H89 inhibited dbcAMP-induced CREB phosphorylation but not dbcAMP-induced Rap1 activation (Figure 3B and 3C), indicating that Rap1 activation does not depend on PKA, whereas CREB phosphorylation depends exclusively on PKA. We next tested whether Rap1 activation and CREB phosphorylation are induced by 8CPT, which has been developed recently as a specific activator for Epac.[25] 8CPT only activated Rap1, not CREB. In striking contrast, 6Bnz induced CREB activation but did not affect

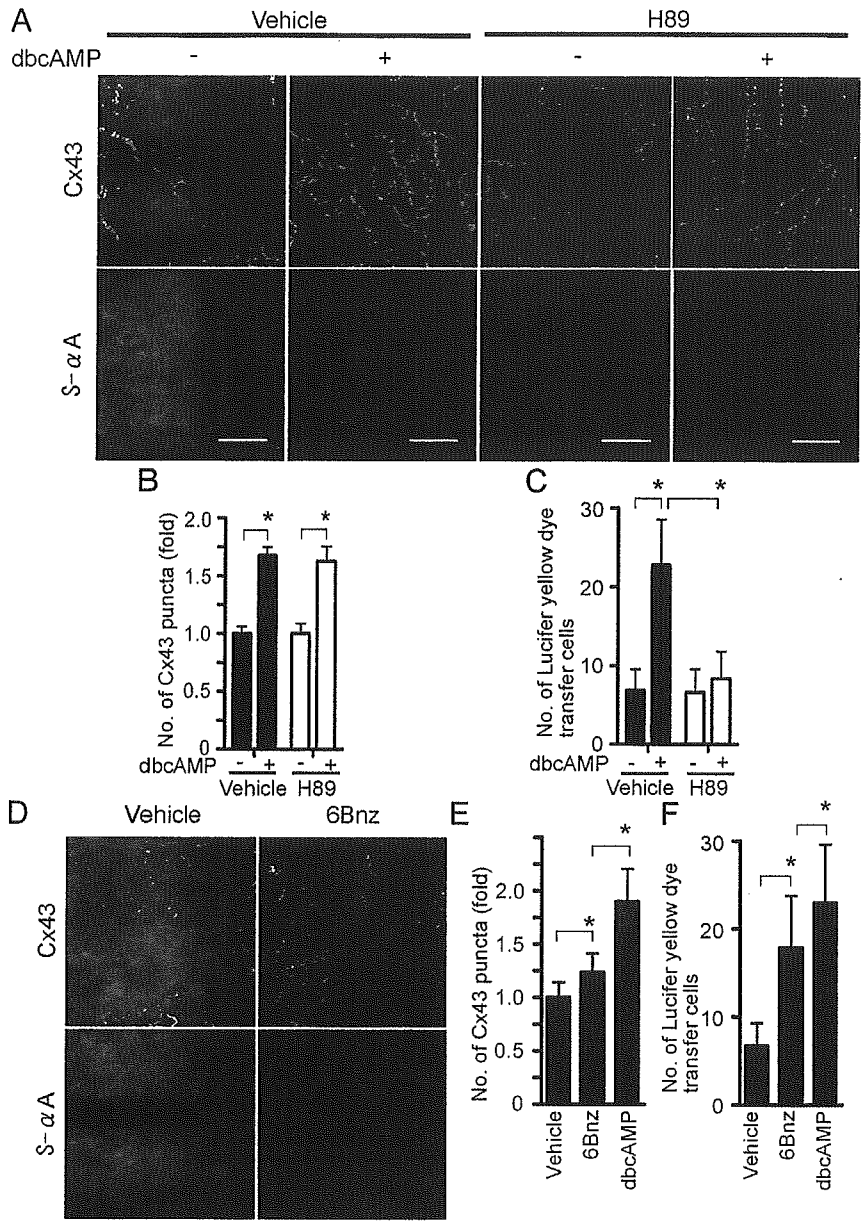

Figure 2. PKA signaling mainly contributes to gating function of GJs. A, NRCMs pretreated with or without 5 μmol/L H89 for 30 minutes were stimulated with or without 1 mmol/L dbcAMP in the presence or absence of 5 μmol/L H89 for 12 hours. After the stimulation, cells were immunostained with anti-Cx43 and anti-S-αA as described in Figure 1A legend. Bar=20 μm. B, Cx43 accumulation in cells treated as in A was quantitatively analyzed. Statistical significance between groups was analyzed by two-way ANOVA with Scheffe's method, indicating that the factor of with/without dbcAMP is significant but not that of vehicle/H89 (*P<0.05; n=6) C, Effect of H89 on dbcAMP-enhanced gap junctional intercellular communication was evaluated by microinjected dye transfer assay as described in Figure 1E legend. Statistical significance between groups was analyzed by two-way ANOVA with Scheffe's method, indicating that both factors, with/without dbcAMP and vehicle/H89, are significant (*P<0.05; n=6). D, NRCMs were stimulated with either vehicle or 1 mmol/L 6Bnz for 12 hours and immunostained with anti-Cx43 and anti-S-αA. Bar=20 μm. E, The effect of 1 mmol/L 6Bnz on Cx43 accumulation at the cell–cell contacts was evaluated similarly to Figure 1B. Statistical significance between groups was analyzed by one-way ANOVA with Scheffe's method (*P<0.05; n=4). F, The effect of 6Bnz on junctional intercellular communication between NRCMs was similarly evaluated by microinjected dye transfer assay to the Figure 1D. Statistical significance was evaluated by one-way ANOVA with Scheffe's method (*P<0.05; n=4).

Rap1 activity (Figure 3D and 3E). Together, these findings demonstrate that cAMP activates Epac-Rap1 and PKA signaling pathways in NRCMs.

Activation of Epac Signaling Leads to Cx43 Accumulation at Cell–Cell Contacts

Because we observed Rap1 activation in response to dbcAMP, we proceeded to investigate the involvement of Epac-Rap1 signaling in cAMP-induced Cx43 accumulation at cell–cell contacts. Like dbcAMP, 8CPT significantly enhanced the accumulation of Cx43 at the cell–cell contacts (Figure 4A and 4B). 8CPT induced Cx43 accumulation at the cell–cell contacts to a similar extent to dbcAMP and to a greater extent than 6Bnz. 6Bnz only slightly increased the number of Cx43 puncta (Figure 4B) compared with vehicle and did not further increase the accumulation of Cx43 at cell–cell contacts caused by 8CPT alone. These results indicate that Epac-mediated signaling is mainly responsible for cAMP-induced Cx43 accumulation at the cell–cell contacts.

We excluded the possibility that increased synthesis of Cx43 on cAMP stimulation resulted in the accumulation of Cx43 at the cell–cell contacts. No discernible increase was observed in the cells stimulated with vehicle, dbcAMP, 8CPT, 6Bnz, and a combination of 8CPT and 6Bnz for 12 hours (Figure 4C and 4D), suggesting that distribution or functional augmentation of GJs is essential for cAMP-induced functional GJ neoformation. In addition, phosphorylation of Cx43 was not affected by dbcAMP, 8CPT, or 6Bnz, nor a combination of 8CPT and 6Bnz (Figure 4C and 4E).

Epac Enhances AJ Formation

Several lines of evidence suggest that AJ formation organized by N-cadherin is a prerequisite for GJ assembly in cardiomyocytes when reassembling and recoupling.[26–28] We used reassembling NRCMs before drug treatment. Recently, we and others revealed that Rap1 is involved in the cell–cell contacts mediated by epithelial (E)-cadherins and vascular

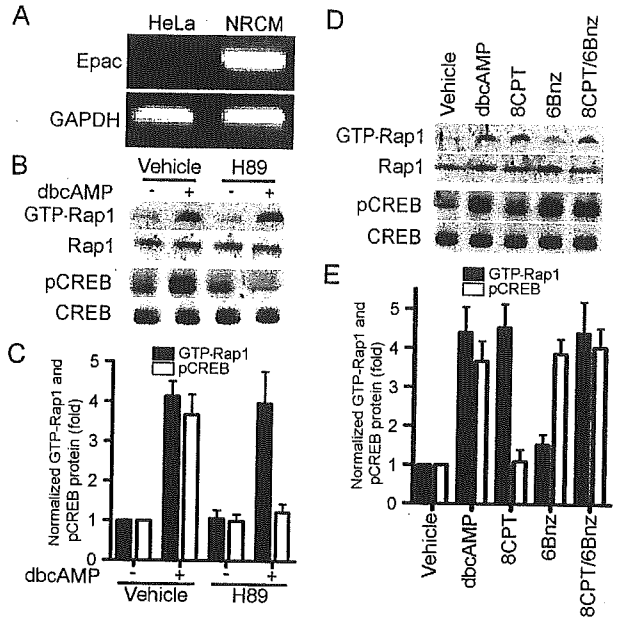

Figure 3. cAMP induces Epac-Rap1 signal as well as PKA signal in NRCMs. A, RT-PCR analysis shows the expression of Epac in NRCMs but not in HeLa cells (used as a negative control). GAPDH was shown as a positive control for RT-PCR. B, Serum-starved NRCMs were stimulated with 1 mmol/L dbcAMP in the absence or presence of H89 for 15 minutes. GTP-bound Rap1 were assessed by pull-down assay. Phosphorylation of CREB was analyzed by Western blot analysis using anti-CREB and anti-phospho-CREB (pCREB). A representative result of 3 independent experiments is shown. C, Data obtained from 4 independent experiments were analyzed quantitatively. Fold activation indicates the ratio of the poststimulation GTP-Rap1 and pCREB intensity of total Rap1 and CREB intensity to the prestimulation GTP-Rap1 and pCREB intensity of total Rap1 and CREB intensity. D, Serum-starved NRCMs were stimulated with either vehicle, 1 mmol/L dbcAMP, 1 mmol/L 8CPT, 1 mmol/L 6Bnz, or 1 mmol/L 8CPT and 1 mmol/L 6Bnz for 15 minutes. GTP-bound Rap1 and phosphorylation of CREB were assessed as described in B. E, Data obtained from 4 independent experiments were analyzed similarly to C.

endothelial–cadherins (VE-cadherins).[18,29] Thus, it is possible that cAMP enhances GJ neoformation by enhancing N-cadherin–mediated AJ formation preceding the GJ formation in NRCMs. To address this possibility, we investigated whether cAMP induces N-cadherin–mediated AJ formation in NRCMs. N-cadherin distribution at cell–cell contacts was enhanced by dbcAMP and 8CPT, whereas 6Bnz neither affected the distribution of N-cadherin nor enhanced the effect of 8CPT (Figure 5A).

To quantitatively analyze the localization of N-cadherin after drug treatment, we performed a biochemical N-cadherin translocation assay. Because N-cadherin is connected to actin cytoskeleton in maturated AJs, cadherin anchored to actin cytoskeleton can be detected in detergent-insoluble fractions of cell lysates. We found an increase in N-cadherin in Triton X-100–insoluble fraction when stimulated by dbcAMP and 8CPT (Figure 5B). However, 6Bnz did not change either basal- or 8CPT-increased levels of N-cadherin in the Triton X-100–insoluble fraction (Figure 5B and 5C). Collectively, these findings indicate that cAMP enhances AJ formation through Epac in NRCMs. We found no difference in N-cadherin expression in NRCMs stimulated with dbcAMP, 8CPT, or 6Bnz, or a combination of 8CPT and 6Bnz by immunoblotting (data not shown).

Rap1 Activation Is Essential for cAMP-Mediated Cx43 Redistribution and AJ Formation

We investigated the role of Rap1 in cAMP-induced Cx43 accumulation and AJ formation in NRCMs. To examine the effect of Rap1 on AJ and GJ formation, we inactivated Rap1 by adenovirus-expressing Rap1GAP1b, which specifically catalyzes the hydrolysis of GTP to GDP on Rap1.[30] Endogenous Rap1 activity was almost completely suppressed by the expression of increasing amount of Rap1GAP1b in NRCMs (Figure 6A). Moreover, overexpression of Rap1GAP1b inhibited cAMP-induced Rap1 activity without affecting cAMP-stimulated CREB phosphorylation (Figure 6B), confirming that Rap1GAP1b specifically blocks Epac-Rap1 pathway but not PKA-mediated signaling.

Inactivation of Rap1 blocked the cAMP-induced accumulation of Cx43 and N-cadherin at the cell–cell contacts (Figure 6C and 6D). dbcAMP-induced translocation of N-cadherin to cytoskeleton-anchored fraction was inhibited by inactivation of Rap1 but not by LacZ overexpression (Figure 6E and 6F). These results suggest that cAMP induces N-cadherin–based AJ assembly through an Epac-Rap1 signaling pathway, which may precede the accumulation of Cx43-based GJs.

PKA and Epac-Rap1 Signaling Cooperatively Enhances GJ Neoformation in NRCMs

Because we found that PKA alone is not sufficient for cAMP-enhanced GJ neoformation and that Epac-Rap1 signaling is involved in cAMP-induced accumulation of Cx43, we assessed the effect of PKA activation and Epac-Rap1 activation on gating function of GJs. 8CPT merely showed the weak enhancement of the intercellular connection, as revealed by microinjected dye transfer assay (Figure 7A). However, 8CPT significantly enhanced 6Bnz-mediated intercellular communication (Figure 7B). The effect of the combination of 8CPT and 6Bnz was comparable to that of dbcAMP. Given that 8CPT induces the Cx43 accumulation at the cell–cell contacts, cAMP potentiates functional GJ neoformation via a PKA-mediated enhanced gating function and Epac-Rap1 signal-mediated accumulation of Cx43 to cell–cell contacts.

Discussion

The function of GJs in the heart depends on the number of GJs between neighboring cells and the gating function of individual GJ at the cell–cell contacts. We investigated how cAMP induces Cx43 accumulation at cell–cell contacts and enhances gating function in NRCMs that were about to develop the mature cell–cell contacts. For the first time, we demonstrated the involvement of Epac-Rap1 signaling downstream of cAMP in GJ neoformation of cardiomyocytes. Although Cx43 accumulated at the cell–cell contacts on cAMP stimulation has been ascribed to PKA,[7] this study demonstrated that Epac-Rap1 signaling activated by cAMP is mainly responsible for the redistribution of Cx43 to cell–cell contacts.

The number of GJs was increased by Epac-Rap1 downstream of cAMP as indicated by the increase in Cx43-positive puncta at cell–cell contacts. However, there was no increase in the amount of Cx43 after cAMP treatment, indicating the importance of the redistribution of Cx43 rather than increase of Cx43 transcription on cAMP. How does Epac signaling induce the accumulation of Cx43 at cell–cell contacts?

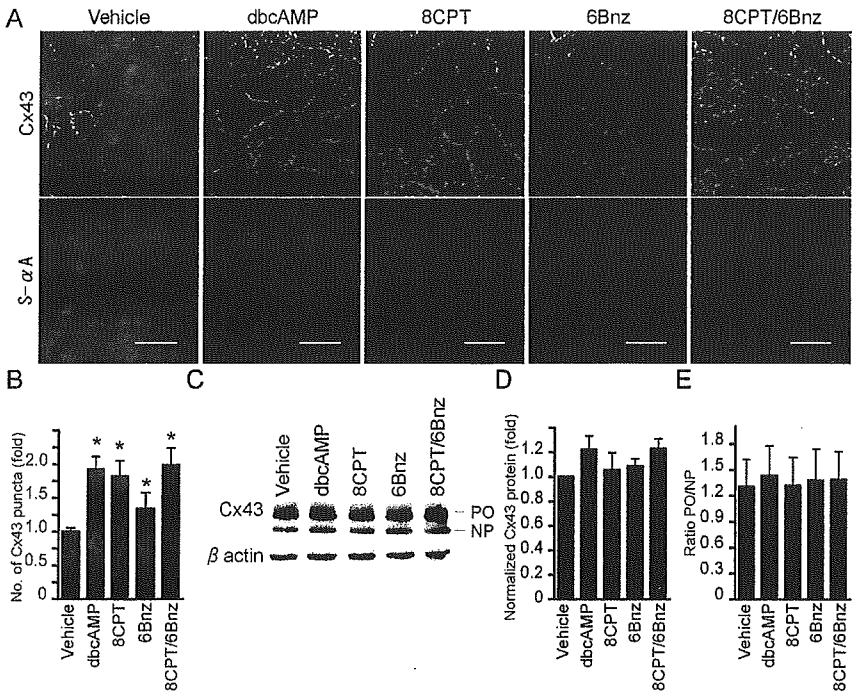

Figure 4. Activation of Epac signaling induces Cx43 accumulation at cell–cell contacts. A, NRCMs stimulated for 12 hours with drugs as indicated at the top were stained with anti-Cx43 and anti-S-αA as described in Figure 1A legend. Bar=20 μm. B, Cx43 accumulation was quantitatively analyzed in Figure 1B. Significant differences between vehicle-treated cells and all drug-treated cells was analyzed by one-way ANOVA with Scheffe's method (*$P<0.05$; n=6). C, NRCMs stimulated as indicated at the top were examined for Cx43 by Western blot analysis. Upper and lower bands correspond to phosphorylated (PO) and nonphosphorylated (NP) Cx43, respectively. D, Total Cx43 (phosphorylated and nonphosphorylated) expression of NRCMs treated for 12 hours with drugs as indicated at the bottom was quantitatively analyzed by three independent Western blot analyses for Cx43. The intensity of the drug-stimulated Cx43 normalized by β-catenin divided by that of vehicle-stimulated Cx43 was expressed as fold activation. E, The ratio is expressed by the intensity of phosphorylated Cx43 (PO) divided by that of nonphosphorylated Cx43 (NP).

Epac-Rap1 activation resulted in enhancement of AJ formation accompanied by GJ formation, as evidenced by increases in N-cadherin and Cx43 at the cell–cell contacts after dbcAMP stimulation (Figure 5). AJ formation constituted by N-cadherin is a prerequisite for GJ neoformation.[28,31] When adult myocytes are cultured, Cx43 is transported and accumulated at the plasma membrane, where N-cadherin accumulates on cell–cell contact.[26] Therefore, GJ formation depends on N-cadherin–based AJ maturation. We have shown previously that the Epac-Rap1 signal enhances the VE-cadherin–based cell–cell contacts in vascular endothelial cells.[18] In this study, we found that Epac activation resulted in the increased accumulation of N-cadherin at the intercellular junction of NRCMs. Thus, N-cadherin accumulation at the cell–cell contacts induced by the Epac-Rap1 signal may account for Cx43 accumulation in NRCMs by analogy to Epac-Rap1–triggered VE-cadherin accumulation in vascular endothelial cells.

The target of activated Rap1 for enhancement of cadherin-based AJ is still unclear. Rac belonging to Rho family GTPase and regulating actin cytoskeleton is suggested to function downstream of Rap1.[32] Therefore, Rac may increase the chances of cell contacts and induce cadherin engagement by extending membrane downstream of Rap1. Maturated N-cadherin on Epac activation, which is detected in the cytoskeleton-anchored fraction, may be accompanied by translocation of Cx43 through cadherin-associating β-catenin

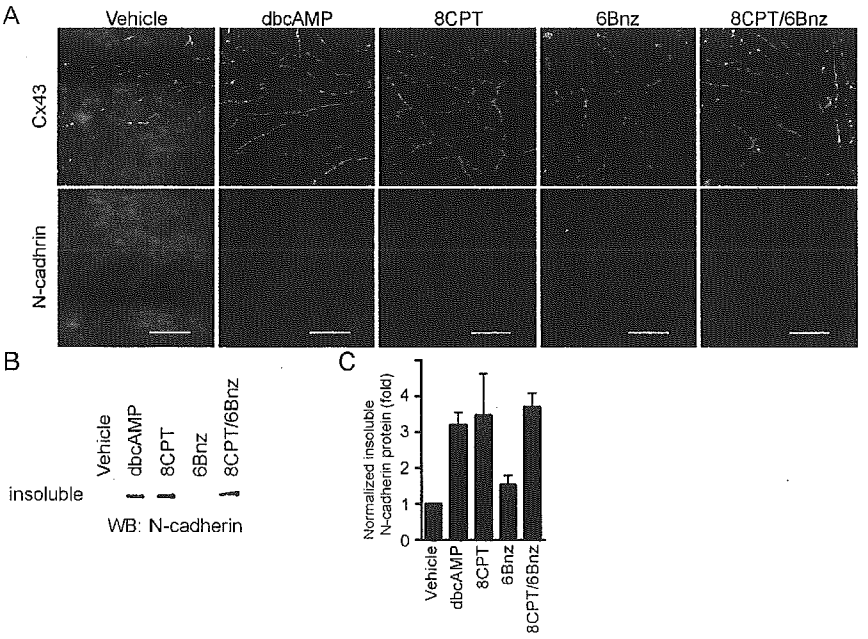

Figure 5. Activation of Epac induces AJ formation. A, NRCMs stimulated for 12 hours with drugs as indicated at the top were immunostained with anti-Cx43 (green) and anti-N-cadherin (red). Bar=20 μm. B, NRCMs stimulated as in A were fractionated with cytoskeleton stabilizing buffer. Triton X-100–insoluble fraction was subjected to SDS-PAGE followed by Western blot analysis (WB) with anti-N-cadherin. A representative result of three independent experiments is shown. C, The data obtained from three independent experiments of B was quantitatively analyzed. The result is indicated as fold increase calculated by dividing the amount of insoluble N-cadherin from the cells treated with the drug by that from the cells treated with vehicle.

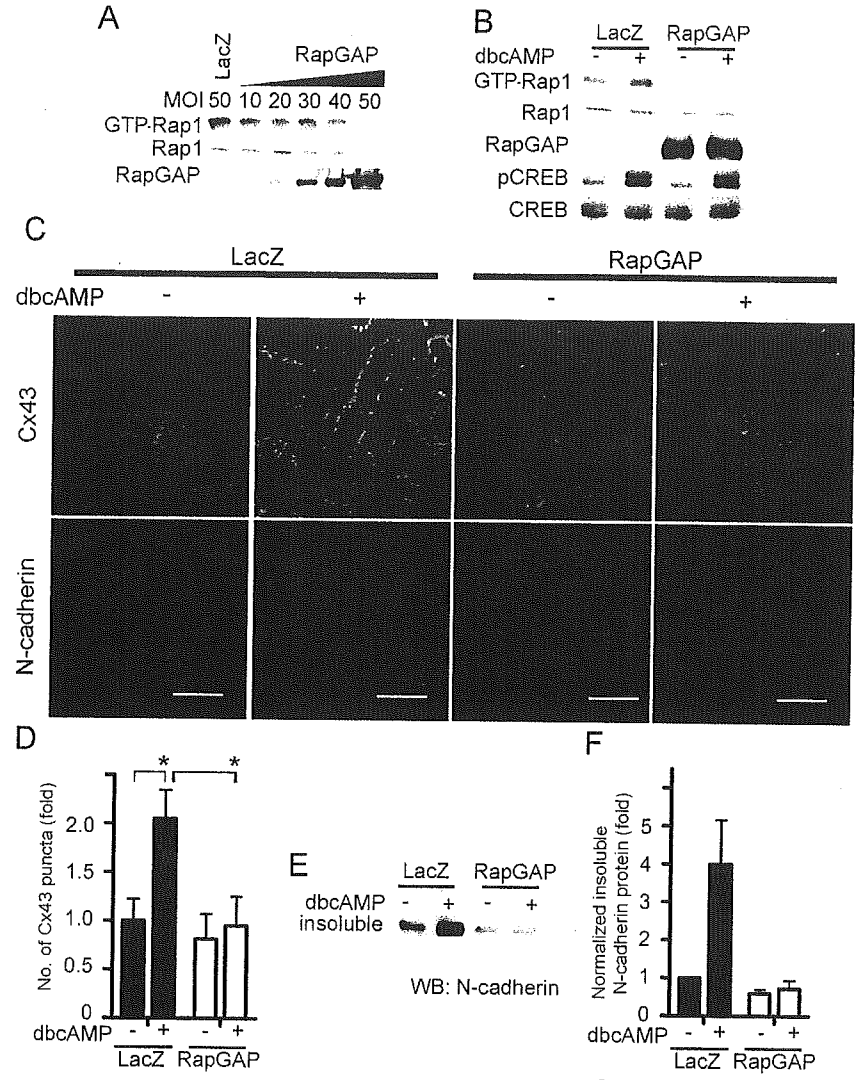

Figure 6. Rap1 activation is required for cAMP-induced Cx43 accumulation at the cell–cell contacts and AJ formation. A, Rap1 inactivation by Rap1GAP1b was verified by detecting GTP-Rap1 in NRCMs infected with different multiplicity of infection (MOI) of adenovirus-expressing Rap1GAP1b (Ad-RapGAP). An adenovirus-expressing LacZ (Ad-LacZ) at 50 MOI was used as a control. GTP-Rap1 was detected by pull-down assay. Rap1 and Rap1GAP1b (RapGAP) expression was examined by Western blot analysis using antibodies as indicated at the left. B, NRCMs infected with either Ad-LacZ or Ad-RapGAP at an MOI of 50 for 24 hours were stimulated with vehicle (−) or 1 mmol/L dbcAMP (+) for 15 minutes and analyzed for Rap1 and CREB activation. C, Localization of N-cadherin and Cx43 was examined similarly to Figure 5A in NRCMs infected with Ad-LacZ or Ad-RapGAP after stimulated with vehicle or 1 mmol/L dbcAMP for 12 hours. Bar=20 μm. D, The effect of inactivation of Rap1 on dbcAMP-induced accumulation of Cx43 was analyzed by two-way ANOVA with Scheffe's method, indicating that both factors, with/without dbcAMP and LacZ/RapGAP, are significant (*P<0.05; n=6). E, Translocation of N-cadherin was examined in NRCMs infected with Ad-LacZ or Ad-RapGAP after stimulation of dbcAMP. A representative of three independent results is shown. F, The three independent results from D were analyzed similarly to Figure 5C.

because Cx43 is capable of binding to β-catenin.[14] Because ZO-1 is recruited to AJs by binding to α-catenin and is also capable of binding to Cx43,[33] ZO-1 may participate in the accumulation of Cx43 during maturation of AJs.

Another factor affecting functional GJ neoformation in addition to the number of GJs is the gating function of individual GJs. PKA activation facilitates intercellular communication without accumulation of Cx43 at cell–cell contacts, concurring with previous reports underpinning that PKA and cAMP increases single channel conductance of the GJ,[34] although the characteristics of single GJ channel conductance evoked by PKA activation still remains elusive.[15]

We found a marked increase in dye transfer on PKA activation with a slightly increased accumulation of Cx43 at the cell–cell contacts (Figures 4 and 7). These results indicate that PKA mainly contributes to the functional neoformation of GJs by enhancing gating function of GJs. Phosphorylation of Cx43 on Ser residues is required for intercellular communication of GJs.[35] Because we found no significant increase in either total Cx43 or phosphorylated Cx43, PKA may indirectly modulate GJ conductance in addition to direct phosphorylation of Cx43 or may phosphorylate a critical Ser/Thr that was indistinguishable in the phosphorylated Cx43 band in our immunoblot for Cx43 (Figure 4C).

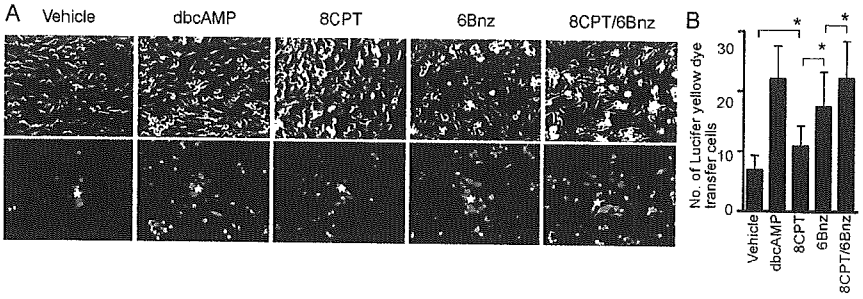

Figure 7. PKA signal and Epac-Rap1 signal cooperatively enhance intercellular communication through GJs. A, Intercellular communication was assessed by microinjected dye transfer assay using NRCMs stimulated with drugs as indicated at the top. B, Dye spread was quantitatively analyzed similarly to Figure 2F. Statistical significance between groups was evaluated by one-way ANOVA with Scheffe's method (*P<0.05; n=6).

The enhanced gating function of GJs is mainly ascribed to PKA, whereas the accumulation of Cx43 to cell–cell contacts is mainly attributable to Epac-Rap1 signal. Hence, Epac-Rap1 signal may accelerate the trafficking of Cx43 to the plasma membrane or inhibit the endocytosis of Cx43 from the plasma membrane. We did not quantify the translocation of Golgi fraction to cell–cell contacts on cAMP stimulation. Previously, GJ trafficking was dynamically monitored by green fluorescence protein–tagged Cx43.[36] Therefore, it will be of great interest to observe the Cx43 dynamics on 8CPT stimulation to directly elucidate Epac-Rap1 signaling.

In conclusion, we demonstrated that cAMP potentiates functional GJ neoformation by a PKA-dependent increase in intercellular communication and by an Epac-Rap1–dependent accumulation of Cx43 in NRCMs.

Acknowledgments

This work was supported in part by grants from the Ministry of Health, Labor, and Welfare Foundation of Japan; the Ministry of Education, Science, Sports, and Culture of Japan; the Promotion of Fundamental Studies in Health Science of the Organization for Pharmaceutical Safety and Research of Japan; the Japan Health Science Foundation; and Astellas Foundation for Research on Metabolic Disorders. We thank Michiyuki Matsuda and Akihiro Umezawa for their helpful input; Nobuo Shirahashi for statistical analysis; James T. Pearson and Michael E. Mendelsohn for critical reading; and Yuko Matsuura and Manami Sone for their technical assistance.

References

1. Yeager M. Structure of cardiac gap junction intercellular channels. *J Struct Biol.* 1998;121:231–245.
2. Sohl G, Willecke K. Gap junctions and the connexin protein family. *Cardiovasc Res.* 2004;62:228–232.
3. Vozzi C, Dupont E, Coppen SR, Yeh HI, Severs NJ. Chamber-related differences in connexin expression in the human heart. *J Mol Cell Cardiol.* 1999;31:991–1003.
4. Davis LM, Rodefeld ME, Green K, Beyer EC, Saffitz JE. Gap junction protein phenotypes of the human heart and conduction system. *J Cardiovasc Electrophysiol.* 1995;6:813–822.
5. Saffitz JE, Kleber AG. Effects of mechanical forces and mediators of hypertrophy on remodeling of gap junctions in the heart. *Circ Res.* 2004;94:585–591.
6. Gutstein DE, Morley GE, Fishman GI. Conditional gene targeting of connexin43: exploring the consequences of gap junction remodeling in the heart. *Cell Commun Adhes.* 2001;8:345–348.
7. Darrow BJ, Fast VG, Kleber AG, Beyer EC, Saffitz JE. Functional and structural assessment of intercellular communication. Increased conduction velocity and enhanced connexin expression in dibutyryl cAMP-treated cultured cardiac myocytes. *Circ Res.* 1996;79:174–183.
8. Paulson AF, Lampe PD, Meyer RA, TenBroek E, Atkinson MM, Walseth TF, Johnson RG. Cyclic AMP and LDL trigger a rapid enhancement in gap junction assembly through a stimulation of connexin trafficking. *J Cell Sci.* 2000;113:3037–3049.
9. Saffitz JE, Laing JG, Yamada KA. Connexin expression and turnover: implications for cardiac excitability. *Circ Res.* 2000;86:723–728.
10. Lampe PD, TenBroek EM, Burt JM, Kurata WE, Johnson RG, Lau AF. Phosphorylation of connexin43 on serine368 by protein kinase C regulates gap junctional communication. *J Cell Biol.* 2000;149:1503–1512.
11. TenBroek EM, Lampe PD, Solan JL, Reynhout JK, Johnson RG. Ser364 of connexin43 and the upregulation of gap junction assembly by cAMP. *J Cell Biol.* 2001;155:1307–1318.
12. Lin R, Warn-Cramer BJ, Kurata WE, Lau AF. v-Src phosphorylation of connexin 43 on Tyr247 and Tyr265 disrupts gap junctional communication. *J Cell Biol.* 2001;154:815–827.
13. Toyofuku T, Yabuki M, Otsu K, Kuzuya T, Hori M, Tada M. Direct association of the gap junction protein connexin-43 with ZO-1 in cardiac myocytes. *J Biol Chem.* 1998;273:12725–12731.
14. Ai Z, Fischer A, Spray DC, Brown AM, Fishman GI. Wnt-1 regulation of connexin43 in cardiac myocytes. *J Clin Invest.* 2000;105:161–171.
15. Schulz R, Heusch G. Connexin 43 and ischemic preconditioning. *Cardiovasc Res.* 2004;62:335–344.
16. Kawasaki H, Springett GM, Mochizuki N, Toki S, Nakaya M, Matsuda M, Housman DE, Graybiel AM. A family of cAMP-binding proteins that directly activate Rap1. *Science.* 1998;282:2275–2279.
17. de Rooij J, Zwartkruis FJ, Verheijen MH, Cool RH, Nijman SM, Wittinghofer A, Bos JL. Epac is a Rap1 guanine-nucleotide-exchange factor directly activated by cyclic AMP. *Nature.* 1998;396:474–477.
18. Fukuhara S, Sakurai A, Sano H, Yamagishi A, Somekawa S, Takakura N, Saito Y, Kangawa K, Mochizuki N. Cyclic AMP potentiates vascular endothelial cadherin-mediated cell-cell contact to enhance endothelial barrier function through an Epac-Rap1 signaling pathway. *Mol Cell Biol.* 2005;25:136–146.
19. Cullere X, Shaw SK, Andersson L, Hirahashi J, Luscinskas FW, Mayadas TN. Regulation of vascular endothelial barrier function by Epac, a cAMP-activated exchange factor for Rap GTPase. *Blood.* 2005;105:1950–1955.
20. Oyamada Y, Zhou W, Oyamada H, Takamatsu T, Oyamada M. Dominant-negative connexin43-EGFP inhibits calcium-transient synchronization of primary neonatal rat cardiomyocytes. *Exp Cell Res.* 2002;273:85–94.
21. Ogita H, Kunimoto S, Kamioka Y, Sawa H, Masuda M, Mochizuki N. EphA4-mediated Rho activation via Vsm-RhoGEF expressed specifically in vascular smooth muscle cells. *Circ Res.* 2003;93:23–31.
22. Doble BW, Chen Y, Bosc DG, Litchfield DW, Kardami E. Fibroblast growth factor-2 decreases metabolic coupling and stimulates phosphorylation as well as masking of connexin43 epitopes in cardiac myocytes. *Circ Res.* 1996;79:647–658.
23. Ohba Y, Ikuta K, Ogura A, Matsuda J, Mochizuki N, Nagashima K, Kurokawa K, Mayer BJ, Maki K, Miyazaki J, Matsuda M. Requirement for C3G-dependent Rap1 activation for cell adhesion and embryogenesis. *EMBO J.* 2001;20:3333–3341.
24. Christensen AE, Selheim F, de Rooij J, Dremier S, Schwede F, Dao KK, Martinez A, Maenhaut C, Bos JL, Genieser HG, Doskeland SO. cAMP analog mapping of Epac1 and cAMP kinase. Discriminating analogs demonstrate that Epac and cAMP kinase act synergistically to promote PC-12 cell neurite extension. *J Biol Chem.* 2003;278:35394–35402.
25. Enserink JM, Christensen AE, de Rooij J, van Triest M, Schwede F, Genieser HG, Doskeland SO, Blank JL, Bos JL. A novel Epac-specific cAMP analogue demonstrates independent regulation of Rap1 and ERK. *Nat Cell Biol.* 2002;4:901–906.
26. Hertig CM, Butz S, Koch S, Eppenberger-Eberhardt M, Kemler R, Eppenberger HM. N-cadherin in adult rat cardiomyocytes in culture. II. Spatio-temporal appearance of proteins involved in cell-cell contact and communication. Formation of two distinct N-cadherin/catenin complexes. *J Cell Sci.* 1996;109:11–20.
27. Kostetskii I, Li J, Xiong Y, Zhou R, Ferrari VA, Patel VV, Molkentin JD, Radice GL. Induced deletion of the N-cadherin gene in the heart leads to dissolution of the intercalated disc structure. *Circ Res.* 2005;96:346–354.
28. Kostin S, Hein S, Bauer EP, Schaper J. Spatiotemporal development and distribution of intercellular junctions in adult rat cardiomyocytes in culture. *Circ Res.* 1999;85:154–167.
29. Hogan C, Serpente N, Cogram P, Hosking CR, Bialucha CU, Feller SM, Braga VM, Birchmeier W, Fujita Y. Rap1 regulates the formation of E-cadherin-based cell-cell contacts. *Mol Cell Biol.* 2004;24:6690–6700.
30. Mochizuki N, Ohba Y, Kiyokawa E, Kurata T, Murakami T, Ozaki T, Kitabatake A, Nagashima K, Matsuda M. Activation of the ERK/MAPK pathway by an isoform of rap1GAP associated with G alpha(i). *Nature.* 1999;400:891–894.
31. Volk T, Geiger B. A 135-kDa membrane protein of intercellular adherens junctions. *EMBO J.* 1984;3:2249–2260.
32. Maillet M, Robert SJ, Cacquevel M, Gastineau M, Vivien D, Bertoglio J, Zugaza JL, Fischmeister R, Lezoualc'h F. Crosstalk between Rap1 and Rac regulates secretion of sAPPalpha. *Nat Cell Biol.* 2003;5:633–639.
33. Itoh M, Nagafuchi A, Moroi S, Tsukita S. Involvement of ZO-1 in cadherin-based cell adhesion through its direct binding to alpha catenin and actin filaments. *J Cell Biol.* 1997;138:181–192.
34. De Mello WC. Impaired regulation of cell communication by beta-adrenergic receptor activation in the failing heart. *Hypertension.* 1996;27:265–268.
35. Duncan JC, Fletcher WH. Alpha-1 connexin (connexin43) gap junctions and activities of cAMP-dependent protein kinase and protein kinase C in developing mouse heart. *Dev Dyn.* 2002;223:96–107.
36. Lauf U, Giepmans BN, Lopez P, Braconnot S, Chen SC, Falk MM. Dynamic trafficking and delivery of connexons to the plasma membrane and accretion to gap junctions in living cells. *Proc Natl Acad Sci U S A.* 2002;99:10446–10451.

Long-Term and Sustained COMP-Ang1 Induces Long-Lasting Vascular Enlargement and Enhanced Blood Flow

Chung-Hyun Cho, Kyung Eun Kim, Jonghoe Byun, Hyung-Suk Jang, Duk-Kyung Kim, Peter Baluk, Fabienne Baffert, Gyun Min Lee, Naoki Mochizuki, Jin Kim, Byeong Hwa Jeon, Donald M. McDonald, Gou Young Koh

Abstract—Vascular enlargement is a characteristic feature of angiopoietin-1 (Ang1)-induced changes in adult blood vessels. However, it is unknown whether tissues having Ang1-mediated vascular enlargement have more blood flow or whether the enlargement is reversible. We have recently created a soluble, stable and potent Ang1 variant, COMP-Ang1. In the present study, we investigated the effects of varied dose and duration of COMP-Ang1 on vascular enlargement and blood flow in the tracheal microvasculature of adult mice and explored a possible mechanism of long-lasting vascular enlargement. We found that COMP-Ang1 administered by adenoviral vector induced long-lasting vascular enlargement and increased tracheal blood flow. In contrast, short-term administration of COMP-Ang1 recombinant protein induced transient vascular enlargement that spontaneously reversed within a month. In both cases, the vascular enlargement resulted from endothelial proliferation. The COMP-Ang1–induced vascular remodeling is mediated mainly through Tie2 activation. Sustained overexpression of Tie2 could participate in the maintenance of vascular changes. Together, our findings indicate that sustained treatment with COMP-Ang1 can produce long-lasting vascular enlargement and increased blood flow. **(*Circ Res*. 2005;97:86-94.)**

Key Words: angiopoietin-1 ■ COMP-Ang1 ■ vascular enlargement ■ blood flow

Angiopoietin-1 (Ang1) is known to be a ligand to Tie2 tyrosine kinase receptor expressed on endothelial cells.[1] Ang1/Tie2 signaling is thought be involved in branching and remodeling of the primitive vascular network and in the recruitment of mural cells during development.[2,3] Transgenic overexpression of Ang1 using the skin-specific keratin-14 promoter produces leakage-resistant and enlarged vessels with an increased number of endothelial cells in skin.[4,5] Gene transfer of Ang1 into ischemic tissues produces notably enlarged blood vessels.[6,7] Baffert et al recently identified that Ang1-induced vascular enlargement could be the result of endothelial proliferation in trachea mucosa.[8] Thus, a cardinal feature of Ang1-induced vascular remodeling is vascular enlargement resulting from endothelial cell proliferation in adult animals.[4–8]

Given that Ang1-induced therapeutic benefits correlated with vascular enlargement in the ischemic tissues,[6,7,9] enhanced blood flow through blood vessels enlarged by Ang1 treatment could provide a great therapeutic benefit to ischemic peripheral tissues. However, it is not known whether the tissues having Ang1-mediated enlarged vessels have more blood flow. In addition, the effective dose and treatment period of Ang1 for inducing effective vascular enlargement is not known. Moreover, it is not known whether Ang1-mediated vascular enlargement regresses when Ang1 stimulation is withdrawn.

We have recently developed a soluble, stable, and potent Ang1 variant, COMP-Ang1.[10] To create this protein, we replaced the amino-terminal portion of Ang1 with the short coiled-coil domain of cartilage oligomeric matrix protein (COMP). COMP-Ang1 is more potent than native Ang1 in phosphorylating the Tie2 receptor and signaling via Akt in primary cultured endothelial cells.[10]

In the present study, we investigated effects of period and dose of COMP-Ang1 on vascular enlargement and tissue blood flow in adult mice and investigated a possible mechanism for long-lasting vascular enlargement induced by long-term and sustained COMP-Ang1. To determine the underly-

Original received March 29, 2005; resubmission received May 10, 2005; revised resubmission received June 8, 2005; accepted June 8, 2005.

From the Biomedical Research Center and Department of Biological Sciences (C.-H.C., K.E.K., G.M.L., G.Y.K), Korea Advanced Institute of Science and Technology, Daejeon, Korea; the Department of Medicine (J.B., H.-S.J., D.-K.K.), Samsung Medical Center and Samsung Biomedical Research Institute, Sungkyunkwan University School of Medicine, Seoul, Korea; the Cardiovascular Research Institute, Comprehensive Cancer Center, and Department of Anatomy (P.B., F.B., D.M.M.), University of California, San Francisco; the Department of Structural Analysis (N.M.), National Cardiovascular Center Research Institute, Suita, Osaka, Japan; the Department of Anatomy (J.K.), College of Medicine, The Catholic University of Korea Seoul; and the Department of Physiology (B.H.J), College of Medicine, Chungnam National University Daejeon, Korea.

Correspondence to Gou Young Koh, Biomedical Research Center, Korea Advanced Institute of Science and Technology, 373-1, Guseong-dong, Daejeon, 305-701, Republic of Korea. E-mail gykoh@kaist.ac.kr

© 2005 American Heart Association, Inc.

Circulation Research is available at http://circres.ahajournals.org DOI: 10.1161/01.RES.0000174093.64855.a6

ing mechanism of COMP-Ang1–stimulated vascular remodeling in adult mice, we focused on the microvasculature of the trachea, which is distinguished by its simplicity and monolayer structure. Our results indicate that long-term and sustained COMP-Ang1 produced by adenoviral delivery of COMP-Ang1 induces a long-lasting vascular enlargement and enhanced blood flow without enhanced pericyte recruitment in adult mice. Long-lasting Tie2 expression could be involved in the long-lasting vascular enlargement and enhanced blood flow.

Materials and Methods

Generation of COMP-Ang1 Recombinant Protein and Ade-COMP-Ang1

Recombinant Chinese hamster ovary cells expressing COMP-Ang1 (CA1–2; production rate, ≈30 mg/L) were established as previously described.[11] Recombinant adenovirus expressing COMP-Ang1 or LacZ was constructed using the pAdEasy vector system (Qbiogene). For additional Materials and Methods, see online data supplement at http://circres.ahajournals.org.

Animals, Treatment, and Measurement of Blood Pressure and Heart Rate

Specific pathogen-free FVB/N mice and Tie2-GFP transgenic mice (FVB/N)[12] were purchased from Jackson Laboratory and bred in our pathogen-free animal facility. Male mice 8 to 10 weeks old were used for this study. Animal care and experimental procedures were performed under approval from the Animal Care Committees of the Korea Advanced Institute of Science and Technology. For protein treatment, 200 μg of COMP-Ang1 recombinant protein or BSA dissolved in 50 μL of sterile 0.9% NaCl was injected daily through the tail vein for 2 weeks. For adenoviral treatment, the indicated amount of Ade-COMP-Ang1, Ade-LacZ, or Ade-sTie2-Fc (generous gift from Drs Gavin Thurston and Ella Ioffe at Regeneron Pharmaceuticals, Terrytown, NY) diluted in 50 μL of sterile 0.9% NaCl was injected intravenously through the tail vein. Systemic blood pressure and heart rate were measured under anesthesia.

Enzyme-Linked Immunosorbent Assay

Approximately 50 μL of blood was obtained from the tail vein into a heparinized capillary tube at the indicated times. ELISA was adopted for precise detection of COMP-Ang1 in plasma.

Immunohistochemical Staining

Mice were anesthetized, perfused with 1% paraformaldehyde in PBS, and several organs including tracheas were removed. Tracheas and ear skins were immunostained as whole mounts, whereas other organs were immunostained as sections. Signals were visualized, and digital images were obtained with a Zeiss Apotome microscope and a Zeiss LSM 510 confocal microscope.

Measurement of Tracheal Tissue Blood Flow

After the mice were anesthetized, a type N flowprobe (Transonic Systems Inc, Ithaca, NY) was placed on tracheal wall along second, third, and forth cartilage rings without applying pressure, as this would occlude the vessels and reduce perfusion in the area of interest. The flowprobe was kept in place on the position of the highest sensitivity by a micromanipulator and connected to a laser-Doppler flowmeter (model BLF21; Transonic Systems Inc), which can measure microcirculation in 1 mm^3 of tissue for real-time assessment of perfusion (mL/min per 100 g of tissue).

Morphometric Measurements and Statistics

Morphometric measurements of the vessel diameters and area densities in mouse trachea were made as previously described.[13] For each trachea, the numbers of PH3-immunopositive endothelial cells, platelet/endothelial cell adhesion molecule (PECAM)-1–immunopositive blood vessels, and desmin/NG2-immunopositive pericytes were measured in 5 regions, each 0.21 mm^2 in area. Values were expressed per millimeter squared. Values presented are mean±SD. Significance of differences between mean was tested by analysis of variance followed by the Student–Newman–Keuls test. Statistical significance was set at $P<0.05$.

Results

Systemic Adenoviral COMP-Ang1 Produces Differential Enlargements of Blood Vessels in Mouse Tracheal Mucosa

For in vivo treatments with COMP-Ang1, we developed a stable Chinese hamster ovary cell line (CA1–2) which produces COMP-Ang1 at ≈30 mg/L. The potency, solubility, oligomerization status, and stability of the COMP-Ang1 produced from CA1–2 are similar to those of COMP-Ang1 produced from COS-7 cells transiently transfected with plasmid vector containing the COMP-Ang1 gene[10] (data not shown). Adult mice were treated with a daily intravenous injection of 200 μg of COMP-Ang1 recombinant protein or BSA through the tail vein for 2 weeks, then blood vessels in the tracheal mucosa were visualized with PECAM-1 immunostaining (Figure 1). Six segments of the microvasculature were distinguished by their position in the vascular hierarchy and differences in endothelial cell morphology.[14] Enlargement of tracheal blood vessels was found in mice that received COMP-Ang1 in the following descending order of effect: postcapillary venules>capillaries>collecting venules>venules>terminal arterioles (Figure 1B). No significant change was noted in segmental arterioles. These phenomena were observed in all individuals of several mouse strains studied (FVB/N, C57BL/6, BALB/c, BALB/c-*nu*, C3H/HeJ). No changes in the sizes or shape of tracheal blood vessels were found in mice that received BSA.

Short-Term and Intermittent Circulating COMP-Ang1 Induces Reversible Enlargement of Postcapillary Venules and Arterioles in Tracheal Vessels

When 200 μg of COMP-Ang1 recombinant protein was injected intravenously into adult male mice, circulating COMP-Ang1 level peaked immediately after injection (≈3.75 minutes), then declined, and returned almost to the control level 3 to 4 hours after treatment (Figure 2A, left). The half-life ($t_{1/2}$) of circulating COMP-Ang1 was 11.8 minutes. Daily intravenous injection of 200 μg of COMP-Ang1 for 1 week in mice produced an ≈2.0-fold enlargement of postcapillary venules and a 1.4-fold enlargement of terminal arterioles in the trachea (Figure 2). The COMP-Ang1–induced enlargement of postcapillary venules, collecting venules, venous end of capillaries, venules, and terminal arterioles were further increased up to 2 weeks on continuation of daily injection of COMP-Ang1 for up to 2 weeks. However, COMP-Ang1–induced enlarged blood vessels returned gradually to normal after discontinuation of the COMP-Ang1 treatment (Figure 2). One month after discontinuation of the COMP-Ang1 treatment, a second round of treatment with a daily intravenous injection of 200 μg of COMP-Ang1 for 2 weeks induced similar enlargements